Supporting Information

Glycerol Transport through the Aquaglyceroporin GlpF: Bridging Dynamics and Kinetics with Atomic Simulation

Dong-Dong Wang[a], Jing-Wei Weng[a]*, Wen-Ning Wang[a]*

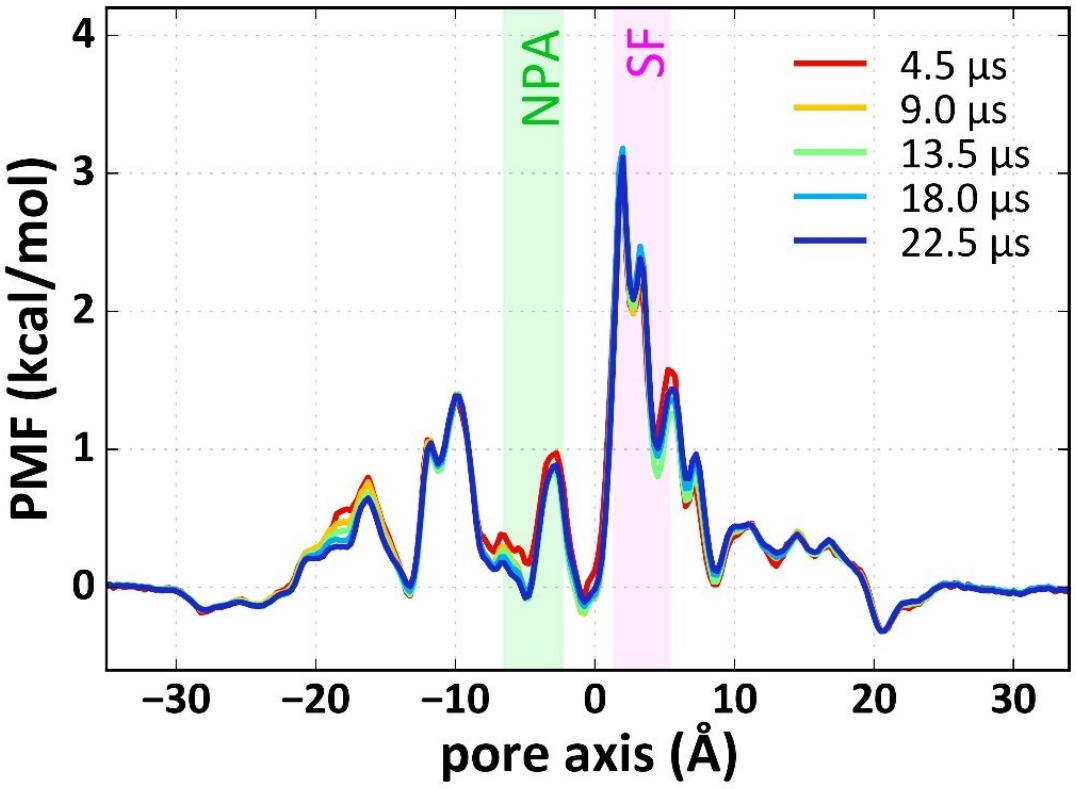

Figure S1. Convergence of the MD simulation. MFs of glycerol moving along the pore axis derived from trajectories of various aggregate simulation times.

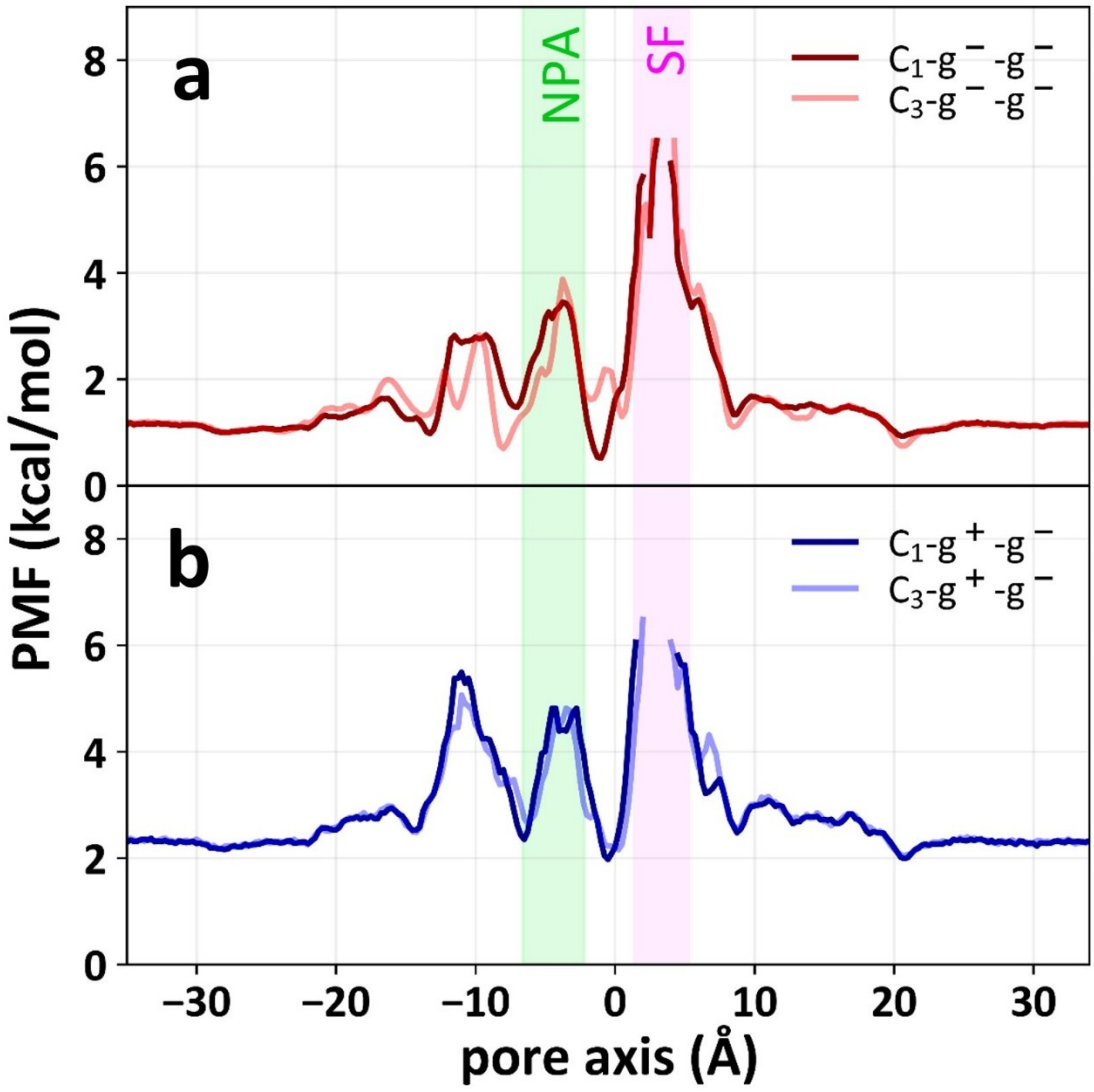

Figure S2. State−dependent PMFs of different conformational and prochiral states of glycerol. (a) PMFs of the C_1–g^-–$g^-$and the C_3–g^-–g^- conformers along the pore axis. (b) PMFs of the C_1–g^+–g^- and the C_3–g^+–g^- conformers. The zero points of the individual PMFs are defined similarly as described in Fig. 3c. Eight state-dependent PMFs are shown here or in Figure 3c and the other ten state-dependent PMFs are of even higher energy and are impermeable at the SF region, thus are not demonstrated.

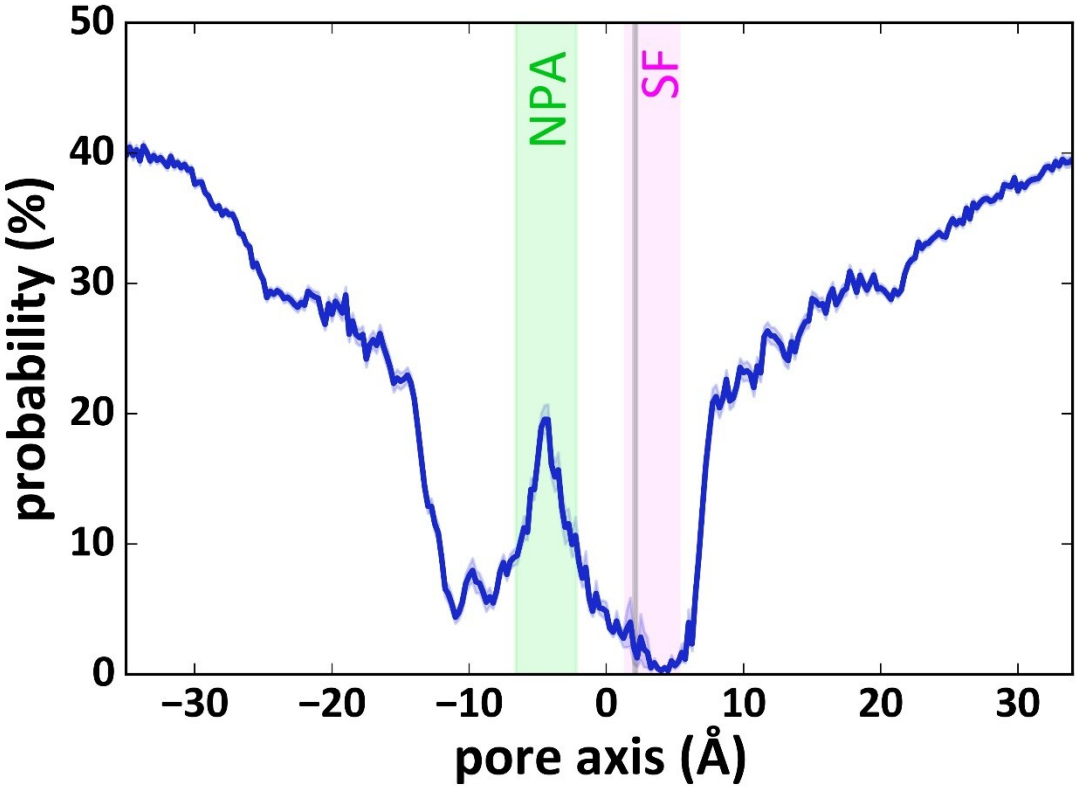

Figure S3. Inter−state transition probability after a time span of 10 ps *versus* the position of glycerol along the pore. The inter−state transition probability is defined as the probability of a glycerol adopting a different conformational or orientational state after 10 ps.

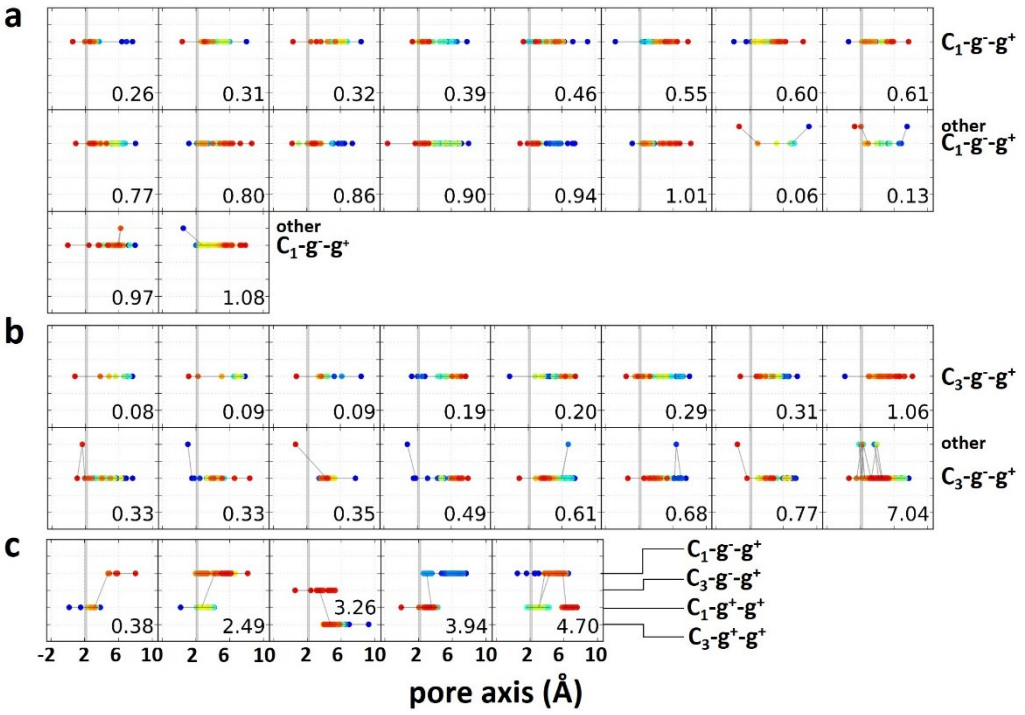

Figure S4. Projections of 39 successful passages through the major barrier region centered at the SF on the 2−dimensional space spanned by the position of glycerol along the pore axis and the conformational and orientational state of the glycerol. (a) Passages during which the C_1–g^-–g^+ conformer overwhelmingly predominates. (b) Passages during which the C_3–g^-–g^+ conformer overwhelmingly predominates. (c) Passages during which the C_1–g^+–g^+ or the C_3–g^+–g^+ conformer appears. Each circle represents one snapshot and is colored time−dependently from blue to red as time elapsed. The neighboring circles are connected by light grey lines. The period from latest entering of glycerol into the region until leaving from the other side is plotted. The number at the bottom−right corner of each panel indicates the time span of the passage in unit of nanoseconds. The "other" row includes both orientors of all the conformers other than g^-–g^+ and g^+–g^+. The grey vertical line denotes the position of the SF barrier in the integrated PMF (z = 2.0 Å).

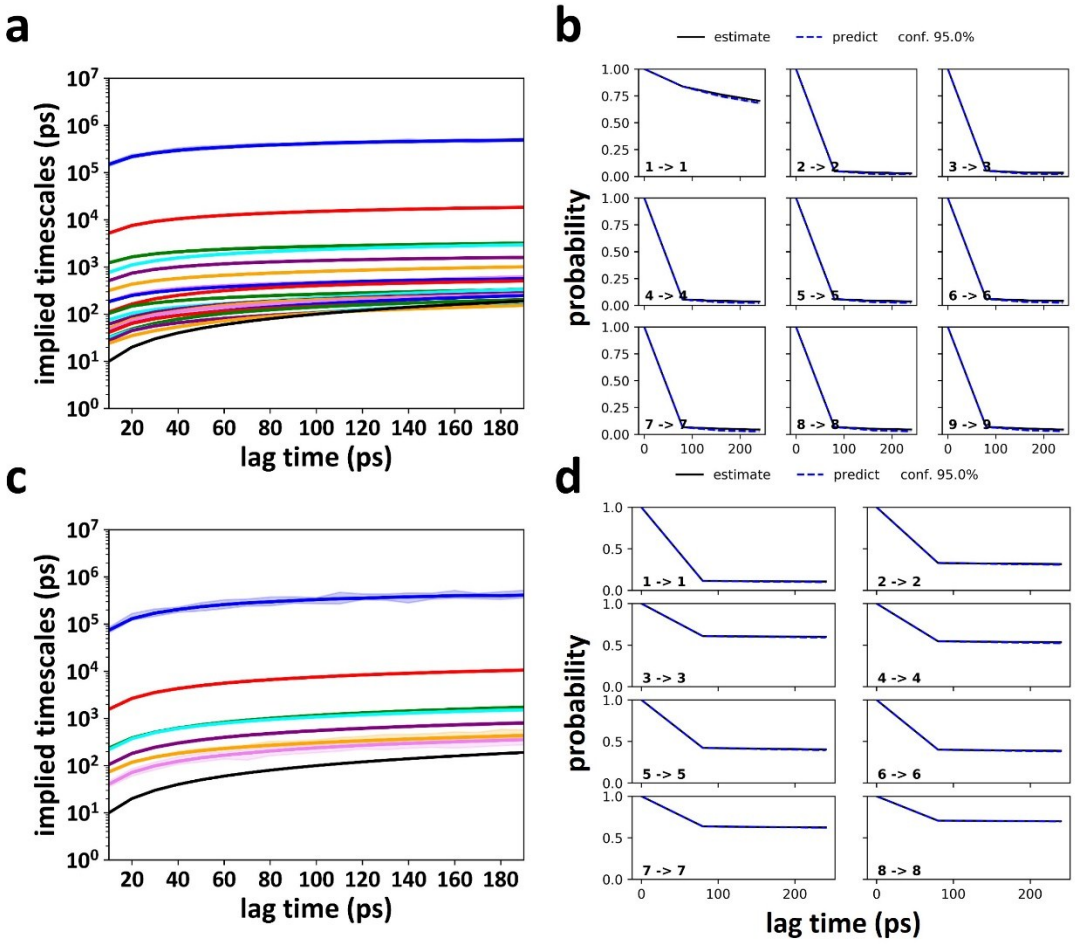

Figure S5. MSM validation. Implied timescales as a function of the lag time of microstates (a) and macrostates (c) show that a lag time τ = 80 ps guarantees Markovian behavior. Shaded regions are 95% confidence intervals. Chapman-Kolmogorov tests of the 202-microstate MSM (b) and the 8-macrostate MSM (d) show that the τ = 80 ps model accurately predicts the residence probabilities on longer time scales.

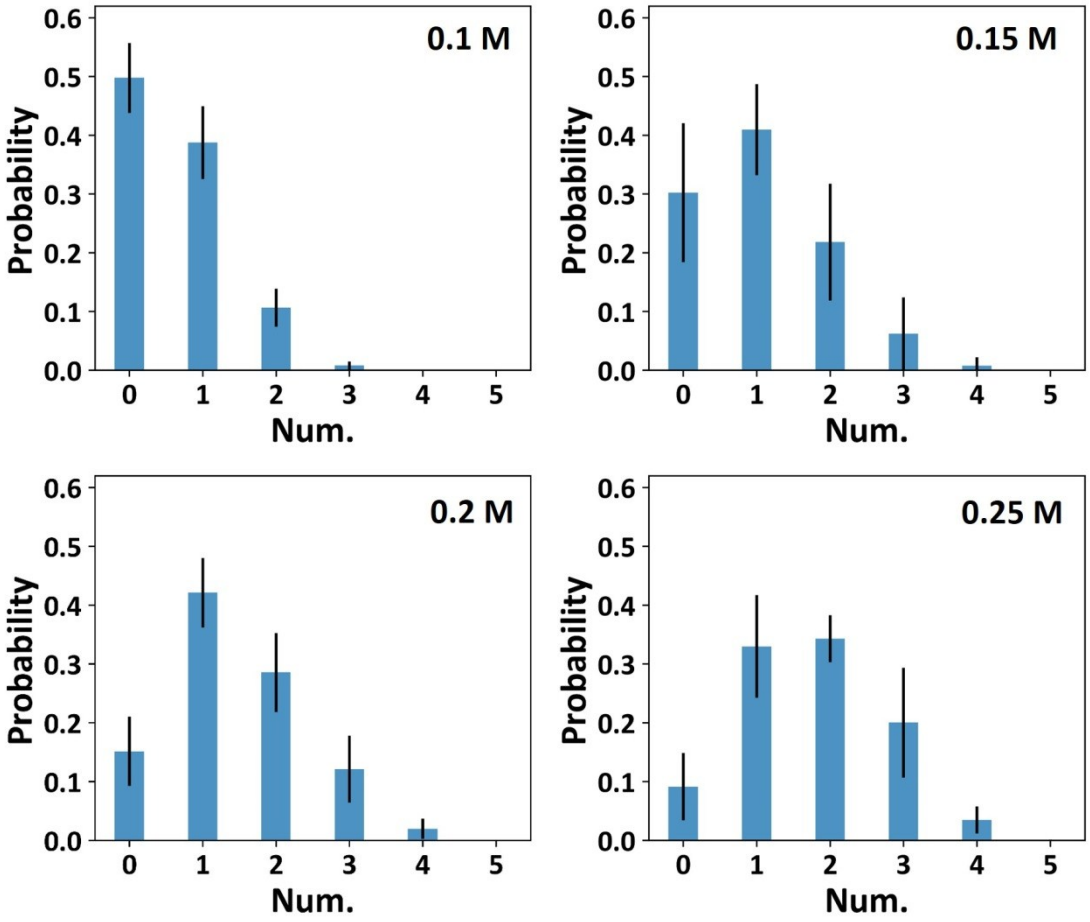

Figure S6. Statistics of the number of simultaneously occupied sites inside the channel. The error bars were estimated based on five independent trajectories.

Table S1. Summary of the dwell time of spontaneous glycerol conduction events. Direction of glycerol translocation: 1 = from the periplasm to the cytoplasm, 0 = from the cytoplasm to the periplasm.

t_{dwell} (ns)	direction [p→c]	t_{dwell} (ns)	direction [p→c]
30.2	1	21.5	0
15.9	1	43.6	0
58.7	1	24.2	0
36.1	1	33.6	0
15.5	1	80.5	0
79.8	1	44.8	0
14.5	1	86.5	0
10.0	1	19.6	0
28.2	1	98.6	0
39.9	1		
63.9	1		
20.3	1		
34.8	1		
46.0	1		
18.2	1		

Table S2. The rate constants of the transitions between the eight macrostates obtained from the 202-state Markov model.

state	population	direction [p→c]	rate constant (ns^{-1})	direction [c→p]	rate constant (ns^{-1})
0	0.2739	k_{01}	17.9993 ($M^{-1}ns^{-1}$)	k_{10}	0.2996
1	0.1104	k_{12}	0.1595	k_{21}	0.1168
2	0.0562	k_{23}	0.0281	k_{32}	0.0342
3	0.0045	k_{34}	0.0023	k_{43}	0.0018
4	0.0670	k_{45}	0.0670	k_{54}	0.0634
5	0.0877	k_{56}	0.0354	k_{65}	0.0466
6	0.1250	k_{67}	0.2057	k_{76}	12.7730 ($M^{-1}ns^{-1}$)
7	0.2753				